Lidar observations of the middle atmospheric thermal tides at Mauna Loa (19.5°N): Comparison with HRDI and GSWM.

Thierry Leblanc [a], I. Stuart McDermid [a], David A. Ortland [b]

[a] JPL, California Institute of Technology, Table Mountain Facility, Wrightwood, CA 92397

[b] **** Ortland address ****

ABSTRACT

The tidal signature in the middle atmospheric thermal structure (15-95 km) at Mauna Loa, Hawaii, (19.5°N) is investigated using more than 145 hours of nighttime lidar measurements obtained during October 3-16, 1996 and October 2-11, 1997. The daytime HRDI temperatures taken in September and October 1993-1997 and zonally averaged at the same latitude are also used. The nighttime lidar and daytime HRDI temperature evolution and tidal signatures are compared to the predictions of the GSWM tidal model. Agreement is found between lidar and GSWM below 60 km, and between HRDI and GSWM above 85 km. Some significant disagreement is found between 60 and 80 km altitude. In particular, a strong semidiurnal signature is observed by lidar and not predicted by GSWM. It appears that the tidal structure observed by lidar is more representative of that predicted by GSWM at 24°N, suggesting a latitudinal shift between theory and observation. It is not clear whether this shift is related to an indetermination of the tidal source and/or propagation or if the observed differences are simply due to local/regional Local-Solar-Time-related oscillations obscuring the tidal signature.

Keywords: lidar, temperature, tides, middle atmosphere, mesosphere.

1. INTRODUCTION

The atmospheric response to the 24-hour periodic solar heating has been observed and studied for decades now. The very first observations recorded on a long-term basis included the diurnal (period of 24-hours) and semidiurnal (period of 12-hours) pressure variations on the ground. Then, using many instrumental techniques and using the classical tidal theory [1, 2] it has been found that even larger variations in pressure, density, temperature and wind would occur in the middle atmosphere, especially above 80 km. Although the Fourier decomposition of the global atmospheric response to a 24-hour periodic forcing theoretically provides a 24-hour component plus all its sub-harmonics (12-hour, 8-hour, etc.), the diurnal and semidiurnal components remain the dominant tidal periods in the entire middle atmosphere (10-110 km) [3]. The tidal winds have been extensively studied in the Mesosphere-Lower-Thermosphere (MLT) region at almost all latitudes. In particular, a strong diurnal signature in the zonal wind has been observed at the equator and in the meridional wind at tropical latitudes with a relatively well defined seasonal cycle [4, 5], and a dominant semidiurnal signature has been observed at mid- and higher-latitudes [6, 7]. In the other hand, very few observations of the thermal tides in the middle atmosphere and MLT region have been performed, mostly due to the lack of reliable instrumental technique for extensively measuring neutral temperature above 60 km altitude. This lack of temperature measurements is even more critical at latitudes lower than 40° when ground-based instruments are particularly sparse. Therefore there is a crucial need for extensive studies on the thermal tides in the stratosphere and mesosphere, especially southward of 30°N, in order to quantify their importance and their role in the middle atmospheric dynamics as well as to better understand the MLT coupling.

This paper presents some results on the middle atmospheric thermal tides obtained from nighttime lidar measurements. A detailed description of the analysis and methodology has been already presented in detail in a study of the tidal signatures observed by lidar above Table Mountain Facility (34.4°N) [8]. The work presented below is a description of the results obtained in October 1996 and 1997 at Mauna Loa Observatory (MLO, 19.5°N). In this study, nighttime temperature profiles (15-100 km) obtained by the Jet Propulsion Laboratory (JPL) Rayleigh/Raman lidar located at MLO [9], and daytime winter temperature profiles (60-110 km) from the High Resolution Doppler Interferometer (HRDI) [10] onboard the Upper Atmosphere Research Satellite (UARS) have been used and compared to the October outputs of the Global Scale Wave Model (GSWM) [11]. The study focuses on the lidar results since the HRDI data set remains statistically limited. After a brief description of the instruments, methodology and data processing, the lidar nighttime and HRDI daytime evolution of the middle atmospheric temperature is compared to its GSWM equivalent. Then estimations of the phases and amplitudes of the diurnal and semidiurnal components are calculated and compared to those of GSWM. A discussion on the points of agreement and disagreement between GSWM and the observations concludes the paper.

2. INSTRUMENTS, DATA SETS, AND DATA PROCESSING.

2.1 Rayleigh and Raman-vibration Lidar temperatures.

Laser radiation transmitted into the atmosphere is backscattered and collected by a telescope. When the Mie scattering due to the aerosols particles is negligible compared to the molecular scattering (i.e. above 30 km) the number of photons received is proportional to the number of photons emitted in the laser pulse and to the number of air molecules (or air density). When the Mie scattering is not negligible (basically below 30 km) the atmospheric relative density can be determined using the vibrational Raman scattering by nitrogen. This scattering is much weaker than Rayleigh scattering but is relatively insensitive to the presence of aerosols, making its use more appropriate at altitudes between 15 and 30 km. For both Rayleigh and Raman scattering methods the temperature is deduced from the relative density using the hydrostatic equilibrium and ideal gas law assumptions. A priori temperature information is needed at the top of the profile and is usually taken from climatological models like CIRA-86. The total error in the temperature at the top due to this a priori initialization can be larger than 20 K but rapidly decreases as the temperature profile is integrated downward (typically divided by a factor of 3 every 10 km). Some description of the Rayleigh/Raman lidar and temperature retrieval techniques and a detailed review of the different sources of temperature uncertainty have been extensively reported [12]. The lidar results described in this paper were obtained using the JPL Rayleigh/Raman lidar located at Mauna Loa Observatory (MLO, 19.5°N, 155.6°W). Due to its low-latitude location and due to the expected seasonal variations of the tides at these latitudes, we focused on the fall equinox. 8 nights from October 3-16, 1996, and 9 nights from October 2-10, 1997 were used, with a maximum of 10 hours of continuous measurements per night. A total of 145 hours of measurements were available, distributed from 19:00 to 5:00 LST.

2.2 HRDI temperatures:

HRDI measures brightnesses in the O_2 atmospheric A band by observing the earth limb with line of sight tangent heights between 50 and 115 km. This brightness is basically proportional to both the band volume emission rate and an emission cross section which is a function of temperature and the emission line within the band. In order to separate the brightness dependence on volume emission rate and temperature, two consecutive limb scans are made in which different lines within the A band are measured. The profiles of brightness measurements from the two limb scans are inverted to provide both a temperature and a band volume emission rate profile [10]. Due to the nature of the viewing modes, temperatures are recovered from 65 to 105 km with the most accurate determinations above 75 km.

To obtain a significant statistical basis, all longitudinally averaged HRDI temperature profiles taken in September and October between 1993-1997 at the latitude of MLO were used. Insufficient information was available from the geographical near-coincidences alone. A total of 72 profiles distributed over 7-hours between 9:00 and 16:00 LST were used for a comparison with the MLO lidar results.

2.3 Data processing:

The first step consisted of taking several nights (days) of lidar (HRDI) measurements during a given season and summing the raw data taken at given Local Solar Times (LST) to obtain mean temperature profiles at given LST. Thus, most of the long-period gravity wave disturbances detected by lidar, most of the variability due to the planetary waves detected by HRDI, and most of the lidar and HRDI instrumental noise, are substantially reduced if not removed. The raw lidar data for each of the 10 long nights of observations obtained between October 3 and 16, 1996 were combined to obtain average nighttime profiles for October 1996, sampled every hour between 19:00 and 5:00 LST. The same method was employed to obtain average nighttime profiles for October 2-11, 1997, and similarly profiles combining October 1996 and 1997. The hourly mean temperature profiles obtained by lidar during the periods of October 1996, October 1997, and both October 1996 and 1997 together are plotted in figure 1. The smoothed aspect of the temperature profiles illustrates the effect of the geophysical and instrumental noise reduction. A temperature minimum is clearly identified at ~80 km in both 1996 and 1997. While the temperature structure below this altitude seems very consistent from a year to another it is not the case at higher altitudes. A maximum temperature difference of ~30 K is observed around 90 km between 1996 and 1997, suggesting a strong interannual variability at this altitude. For the two periods of October 1996 and October 1997 taken separately, and for both periods taken together, the nightly average profile was subtracted from each of the hourly mean profiles. This calculation was also made for the zonally averaged daytime HRDI temperatures obtained at the latitude of MLO in September and October 1993-1997. In the next section, these differences are compared to the corresponding values calculated from the outputs of the Global Scale Wave Model (GSWM). Then the lidar temperature differences were fitted iteratively, using estimations of the tidal phases and amplitudes, to extract both diurnal and semidiurnal components. Some computer simulations of tidal extraction were performed beforehand to insure that the iterative extraction of the 12- and 24-hours components was possible even when using only a 10-11 hour long nighttime measurement window. No such work was attempted for the HRDI differences since the measurement window was only 8 hours.

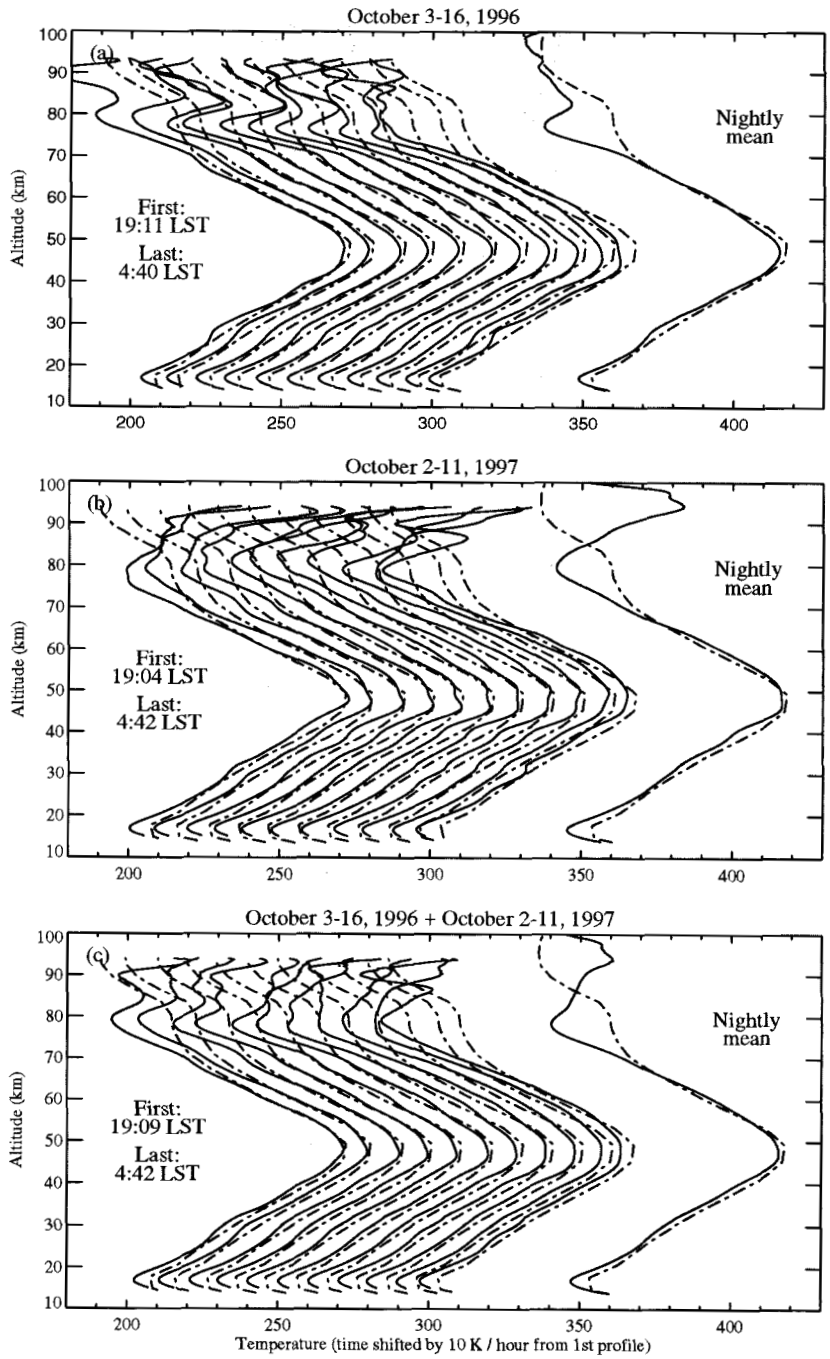

Figure 1. Nighttime evolution of the mean profiles measured by lidar at MLO for the periods of October 3-16, 1996 (a), October 2-11, 1997 (b), and October 1996 and 1997 together (c). The profile on the right side is the nightly mean profiles.

3. DIURNAL EVOLUTION OF TEMPERATURE: COMPARISON WITH HRDI AND GSWM

The temperature differences obtained by lidar every hour between 19:00 and 5:00 LST and by HRDI between 8:00 and 16:00 LST are contoured as a function of altitude and time in figure 2. Due to the limited statistics, the HRDI data cannot be displayed for each year separately and therefore any interannual tidal variability could introduce some small differences between HRDI and lidar. These differences are expected to be negligible compared to the tidal amplitudes and to the residual noise contained in both HRDI and lidar data sets. It should also be noted that the daily-mean temperature and the nightly-mean temperature can be very different, especially in the presence of a strong diurnal component. Moreover the lidar measurements, because of their ground-based character, are expected to be much more sensitive to local/regional effects than

the zonally averaged HRDI measurements. These latter are supposed to be representative of migrating effects only, while the lidar measurements are representative of all migrating, non-migrating, and local/regional effects like gravity waves with periods between 6- and 36-hours. Consequently, a perfect consistency between the observed structures in HRDI differences and in the lidar differences should not be expected unless a strong migrating tidal component is present (i.e. large amplitudes are involved). Actually, a relatively good consistency is observed in figure 2 between the daytime HRDI data and the nighttime lidar data. A warm period is clearly propagating downward from 105 km at 8:00 LST (HRDI) to 70 km at 00:00 LST (lidar), especially well defined in October 1997. The nighttime temperature behavior observed here by lidar between 30 and 80 km has also been observed by lidar over Haleakala, HI (21°N) during the ALOHA-93 campaign [*States and Gardner*, personal communication].

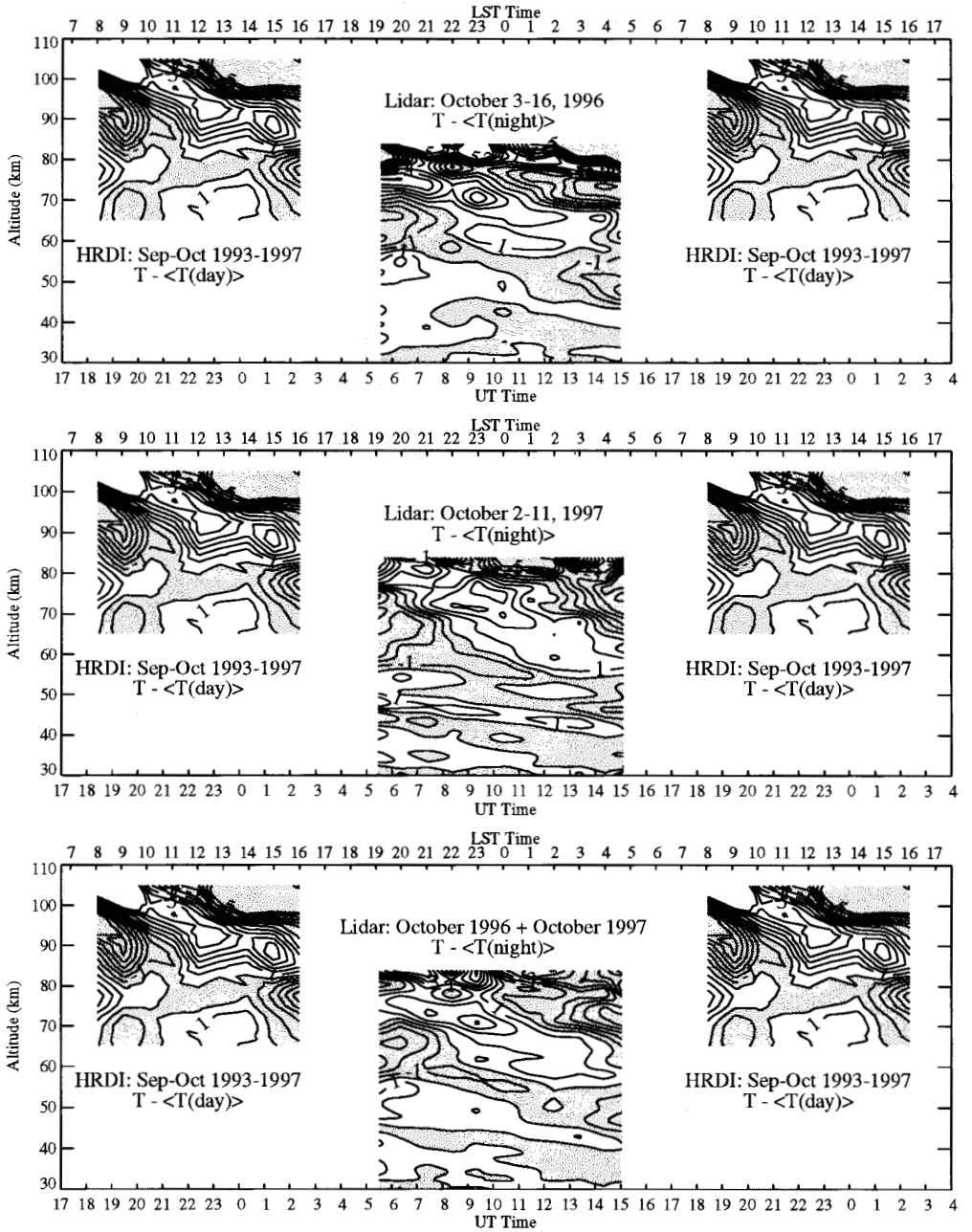

Figure 2. Hourly-mean lidar (HRDI) temperature differences from their nighttime (daytime) average. a) lidar measurements at MLO during October 3-16, 1996, b) October 2-11, 1997, and c) October 1996 and 1997 together. The mean lidar profiles of Figure 1(a) to (c) have been used. For HRDI, all temperature profiles taken at the latitude of MLO in September and October 1993-1997 have been used.

The equivalent GSWM departures from the daytime average and from the nighttime average were calculated. They are plotted in **Figure 3** with the same disposition as in **Figure 2**. Although HRDI and GSWM seem to be in reasonably good agreement above 72 km (aside from a 2.5 hours phase shift), there is a strong disagreement between lidar and GSWM above 60 km. GSWM predicts a cold period at 80-85 km and 22:00-23:00 LST while the lidar observed a warm period at the same time. Also, GSWM predicts a near zero difference from the nightly mean temperature at 70-72 km and 23:00 LST while the lidar observed a clearly warm period. The only point of agreement between GSWM and lidar is located around 50-55 km, with a warmer early night and a colder late night. There is also disagreement between HRDI and GSWM around 70-72 km with a warm period observed by HRDI at 12:00-13:00 LST while a continuous cooling trend during all day is predicted by GSWM. **Figure 3** illustrates very well how different the departure from the nighttime average and the departure from the daytime average can be. In particular, there is no apparent continuity at sunset around 75 k-80 km altitude.

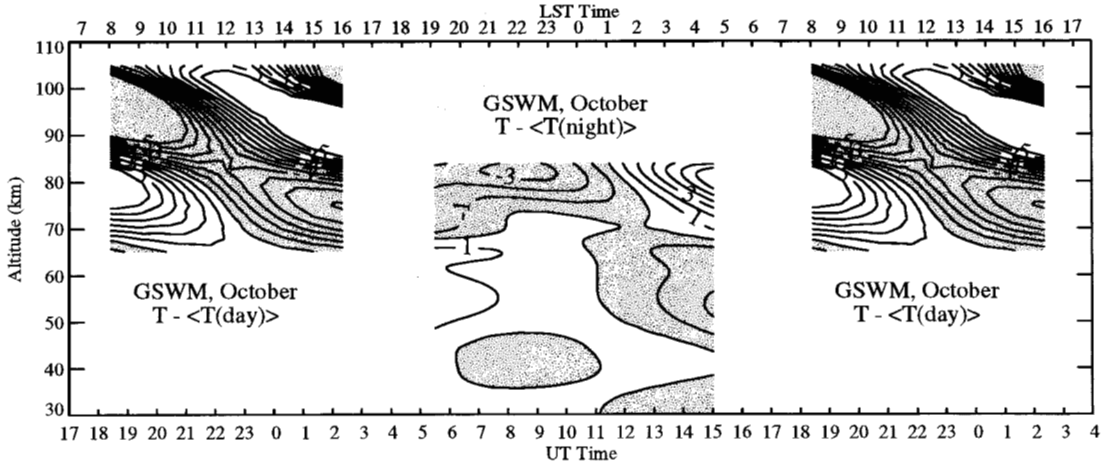

Figure 3. Same as figure 2 but the temperature differences were calculated using the phases and the amplitudes (x2) of the diurnal and semidiurnal components predicted by GSWM at 19.5°N in October.

4. ESTIMATION OF THE DIURNAL AND SEMIDIURNAL COMPONENTS FROM LIDAR MEASUREMENTS.

Figure 4 shows the results of the 2-component fits applied to the GSWM differences from the 10-hour average plotted in figure 3 between 19:00 and 5:00 LST. The true GSWM diurnal and semidiurnal amplitudes are plotted with solid lines and the amplitudes calculated by the fits are plotted with solid lines and error bars. The true GSWM diurnal and semidiurnal phases are plotted with triangles and the phases calculated by the fits are plotted with circles and error bars. Due to the incomplete sampling some regions of constant diurnal phase with height located near 18:00 and 6:00 LST alternate with some regions of undetermined phase located at 12:00 and 00:00 LST [8]. The regions of undetermined phase correspond to a true phase located at 12:00 or 00:00 LST while the regions of constant phase with height associated with a maximum amplitude and minimum standard deviations on amplitude and phase correspond to true phases located at 18:00 or 6:00 LST[8]. Figure 5 is similar to figure 4 but the fit is now applied to the lidar data plotted in figure 2(c) (October 1996 and 1997 together). As already observed when comparing the nighttime evolution of temperature shown in figures 2 and 3, there are some important points of disagreement between the phases and amplitudes observed by lidar and predicted by GSWM above 55 km. The diurnal phase appears to be between 16:00 and 20:00 LST for both lidar and GSWM below 55 km. The region of undetermined diurnal phase observed near 60 km in figure 5 would correspond to an actual phase near 12:00 LST. The diurnal phase predicted by GSWM at this altitude is around 17:00 LST. Also, a region of constant diurnal phase with height at 75-80 km associated with a maximum diurnal amplitude and a minimum standard deviation on the diurnal phase suggest a diurnal phase near 17:00-18:00 LST. At the same altitude, the diurnal phase predicted by GSWM is about 6:00 LST, which is nearly opposite to what is calculated from the lidar observations. An estimation of the correct diurnal phases and amplitudes can be done by comparing with the diurnal phases and amplitudes given by GSWM as a "first guess" [8]. The estimated diurnal phase propagates downward from 17:00 LST at 76 km, to 5:00 LST at 63 km with an associated maximum in amplitude, then 6:00 LST at 59 km and again 18:00 LST at 55 km. It remains constant (~18:00 LST) down to 40 km, as predicted by GSWM. The estimated diurnal phases are in good agreement with the diurnal phases estimated from lidar measurements during ALOHA-93 13. In particular at 70-75 km both observations lead to estimated diurnal phases of 20:00-22:00 LST in total disagreement with the 8:00-9:00 LST predicted by GSWM between 18°N and 21°N. However the amplitudes estimated by Dao remain at least 30% larger than the amplitudes estimated here. The semidiurnal component calculated by the fit seems to

be dominant (or at least of the same order as the diurnal) only at 44-, 59- and 70-km altitude. At these altitudes, the observed phases remain close to the semidiurnal phases calculated by GSWM. Figure 6 is similar to figure 3 but using the newly estimated components instead of GSWM. The agreement is good with both lidar and HRDI, suggesting that the estimations were correctly determined. To ensure this, a 24-hour averaged profile has been estimated and used to re-apply a two-component fit to the lidar data. Using each of the ten hourly composite profiles (from 19:00 to 5:00 LST) and our estimations of the diurnal and semidiurnal phase and amplitude, ten independent 24-hour averaged profiles have been calculated. Then a singular 24-hour averaged profile is obtained by taking the average. If the estimated phases and amplitudes are correct, the newly estimated 24-hour average will be equal or close to each of the 24-hour independent averaged profiles and the results from the fit applied to the departures from this 24-hour average will converge to the true components [8]. As shown in figure 7, the fits have converged to the estimated values, indicating that the estimated 24-hour averaged profile is close to the true profile.

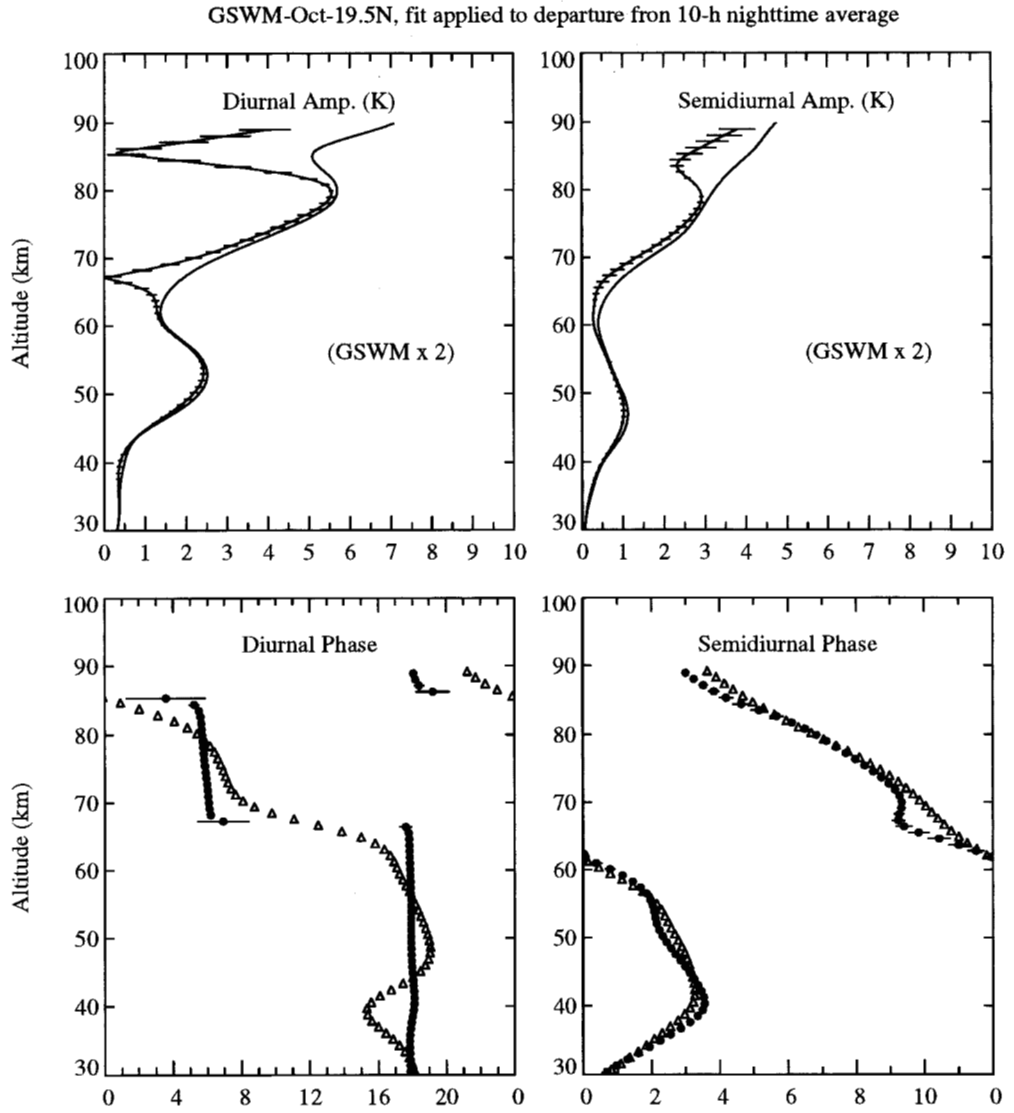

Figure 4. Diurnal and semidiurnal phases (circles with error bars) and amplitudes (solid lines with error bars) calculated by fitting 10 hourly-mean nighttime (from 19:00 to 5:00 LST) temperature profiles (departures from the 10-hour average) as calculated by GSWM at 19.5°N in October. The true GSWM components are plotted with triangles (phases) and solid lines with no error bars (amplitudes x 2).

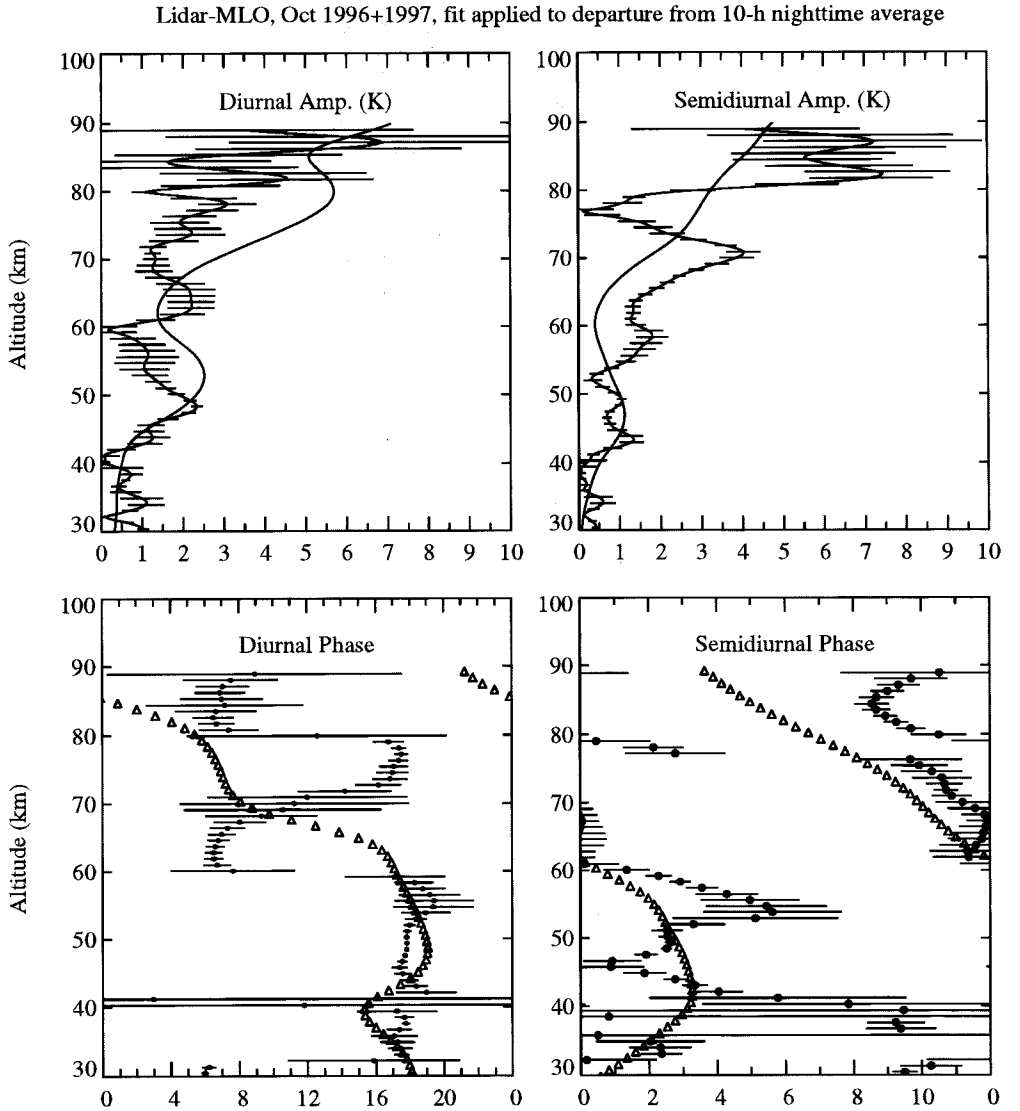

Figure 5. Same as figure 4, but for the MLO lidar temperature differences of October 1996+1997 (see figure 2c)) instead of GSWM. The true GSWM 19.5°N-October phases are plotted with triangles and the amplitudes (x2) with solid lines.

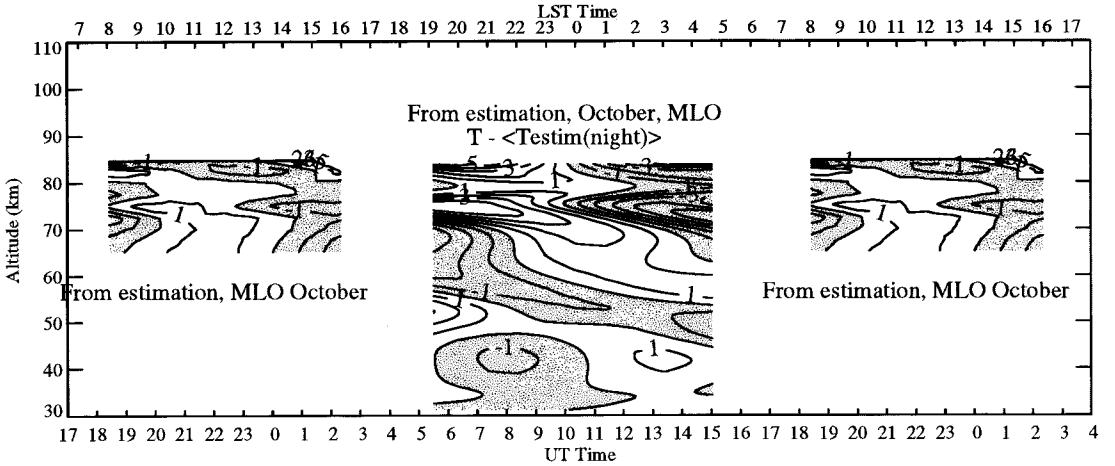

Figure 6. Same as figure 3 but using our own estimated diurnal and semidiurnal phases and amplitudes.

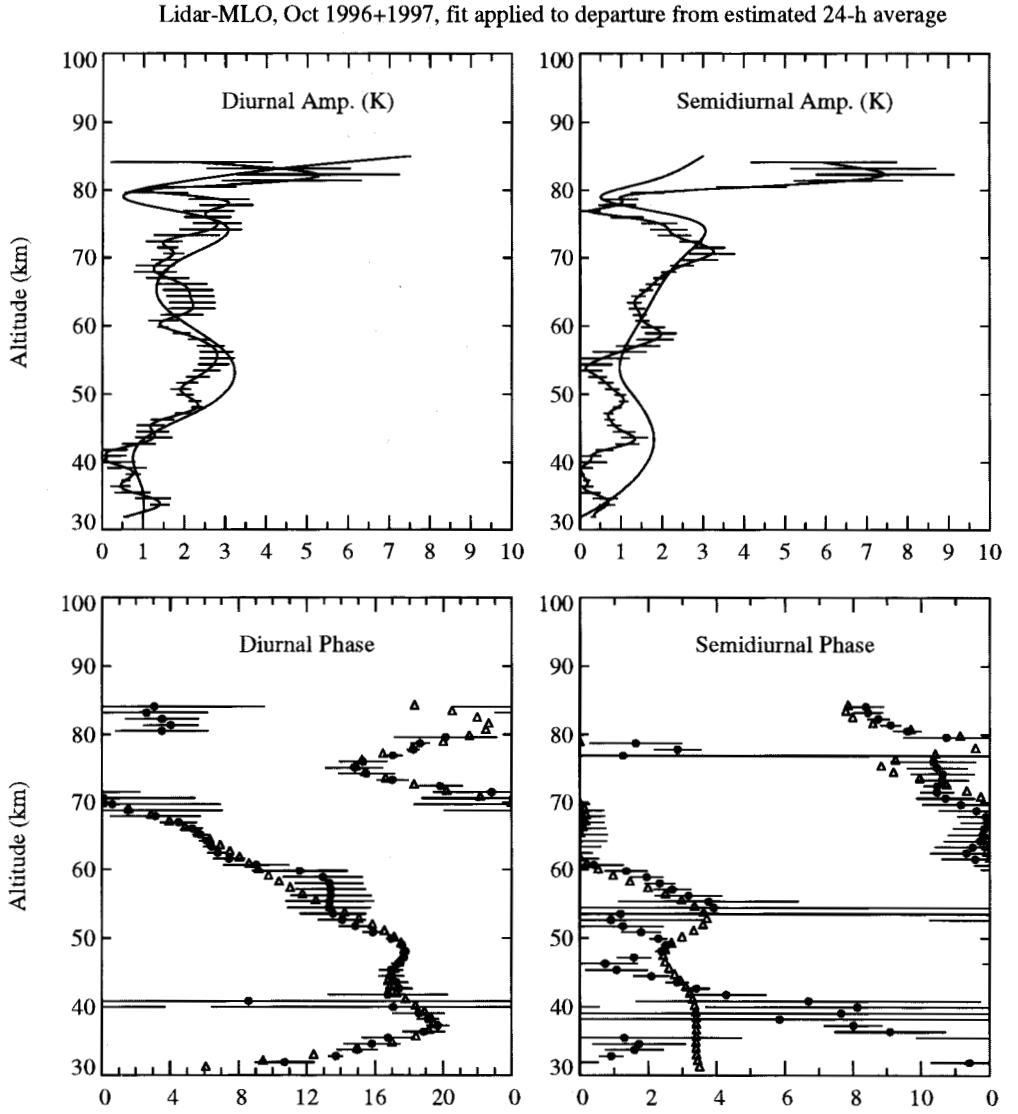

Figure 7. Same as figure 5, but using the differences from our own estimated 24-hour average instead of the actual 10-hour nighttime average. The estimated amplitudes are plotted with solid lines and no error bars and the estimated phases with triangles.

5. DISCUSSION AND CONCLUSION.

The study of the HRDI daytime and lidar nighttime middle atmospheric temperature evolution and its comparison with that predicted by GSWM has led to these principal results:

1) Some consistent LST-related structures have been observed on both HRDI and lidar data suggesting the presence of important migrating tidal components. In particular, a warm period has been clearly identified, propagating downward from 105 km at 8:00 LST to 65 km at 00:00 LST and surrounded by two colder periods above and below.

2) Other LST-related structures have been observed by lidar between 30 and 80 km altitude, consistent with some previous lidar observations at similar latitudes during the ALOHA-93 campaign, in particular a colder early night, warmer midnight, and colder late night around ~70 km suggesting a significant semidiurnal component at this altitude.

3) The comparison with the outputs of the GSWM tidal model has pointed out some similarities but also some disagreement: As previously observed the amplitudes predicted by GSWM are much smaller than that observed by lidar and HRDI. Also the warm downward propagating period described in point (1) is predicted to occur two to three hours later by GSWM compared to the HRDI observations.

4) The main point of disagreement between the lidar observations and GSWM predictions occurs between 60 and 85 km. A large semidiurnal component is observed by lidar leading to early and late cold night and warm midnight while no such large semidiurnal component is predicted by GSWM, leading to an apparent warm early night at 60 km, and an apparent cold midnight at 80 km and above.

A new version of GSWM has been recently released [*Hagan*, personal communication]. This new version (GSWM98) incorporates a recent 5-year wind climatology as background winds. Also the Rayleigh friction in the mesosphere has been modified. When the HRDI and lidar observations are compared to the outputs of GSWM98, the disagreements mentioned in point (3) are substantially reduced above 80 km. The amplitudes predicted by GSWM98 are larger than those predicted by the older version. Also, the phase delay between the warm period propagating downward observed by HRDI (between 105 and 85 km) and predicted by GSWM is mainly removed. However, the large differences between the lidar observations and the GSWM predictions between 60 and 80 km remain. There are several possible explanations for such differences.

A possible explanation is the presence of local/regional effects which may lead to disturbances with periods between 10 and 30 hours. Gravity waves with 12-h or/and 24-h periods may be generated in the convectively active tropical troposphere and propagate upward. A strong diurnal cycle has been observed in the development of tropospheric convection due to the local orography. In particular the Big Island of Hawaii where MLO is located is formed with two high volcanoes, and the oceanic humidity is uplifted on their slopes by the dominant trade winds. After sunset, all the convective clouds (sometimes deep convection clouds) rapidly collapse, leading to clear skies after midnight. This 24-hour periodic pattern is very pronounced in October in Hawaii, and might lead to LST-dependent background winds and temperatures in the middle atmosphere which would consequently disturb the upward propagating tides with a 24-hour repeatability.

Another explanation is related to the latitudinal position of MLO. Figures 8 and 9 are similar to figures 3 and 5 respectively but using the phases and amplitudes predicted by GSWM at 24°N instead of 19.5°N. It is clear that the tidal components change significantly in only 4-5° latitude. The reason is that ~20° latitude is a nodal region for the diurnal component. At 24°N the diurnal phase is located around 18:00 LST at 75 km instead of 7:00 LST at 19.5°N. Also the semidiurnal amplitude is 50% larger especially at 80 km and above. The resulting temperature departures from the nighttime average is still not in perfect agreement with the observations but much is more consistent. This would indicate that GSWM is latitudinally inaccurate. Several mechanisms may account for this uncertainty. First, some contribution from higher modes (with higher latitudinal variability) might be underestimated by GSWM. Theoretically, the (1,1) and (2,2) modes are believed to be less affected by dissipation than the higher modes. Also, the latitudinal structure of the tidal modes (Hough modes for temperature) is believed to be distorted by the background winds. An approximate picture of the background winds in the tropics (in particular a shift by a few degrees latitude) might lead to non-negligible departures from the theory.

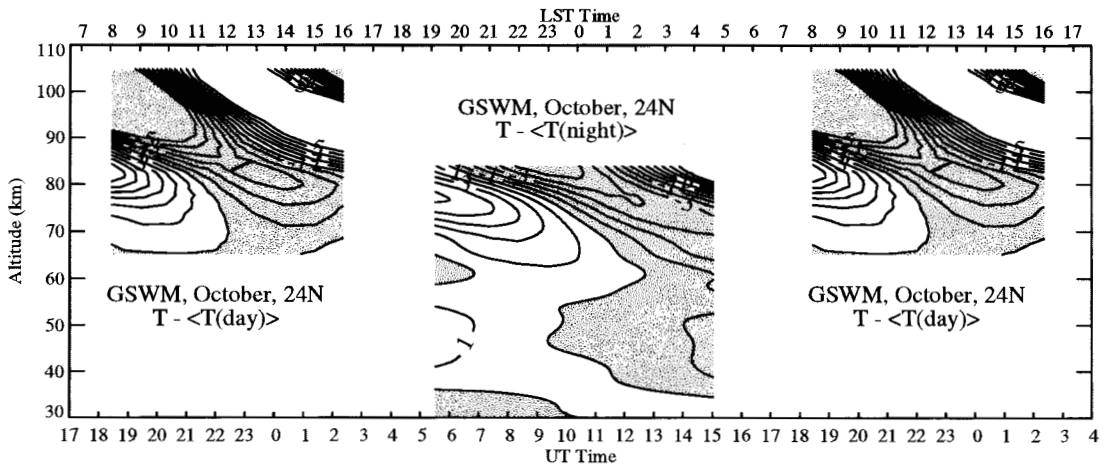

Figure 8. Same as figure 3, but using the phases and amplitudes predicted by GSWM at 24°N.

Some other mechanisms like the effect of diurnal variations of ozone, gravity-wave-tides interaction or tidal wave dissipation are among the candidates. Also, some recent numerical modeling has shown that latent heat released in the troposphere is a non-negligible source of tidal oscillations. More investigations based on both observation and modeling are needed to give a more detailed explanation of the observed differences. The increased number of sophisticated tidal and General Circulation Models (GCM) together with the results from additional full-night lidar campaigns (another campaign is planned at MLO in

October 1998) might give some elements of answers in the future and contribute to a better understanding of the role of the thermal tides in the middle atmosphere.

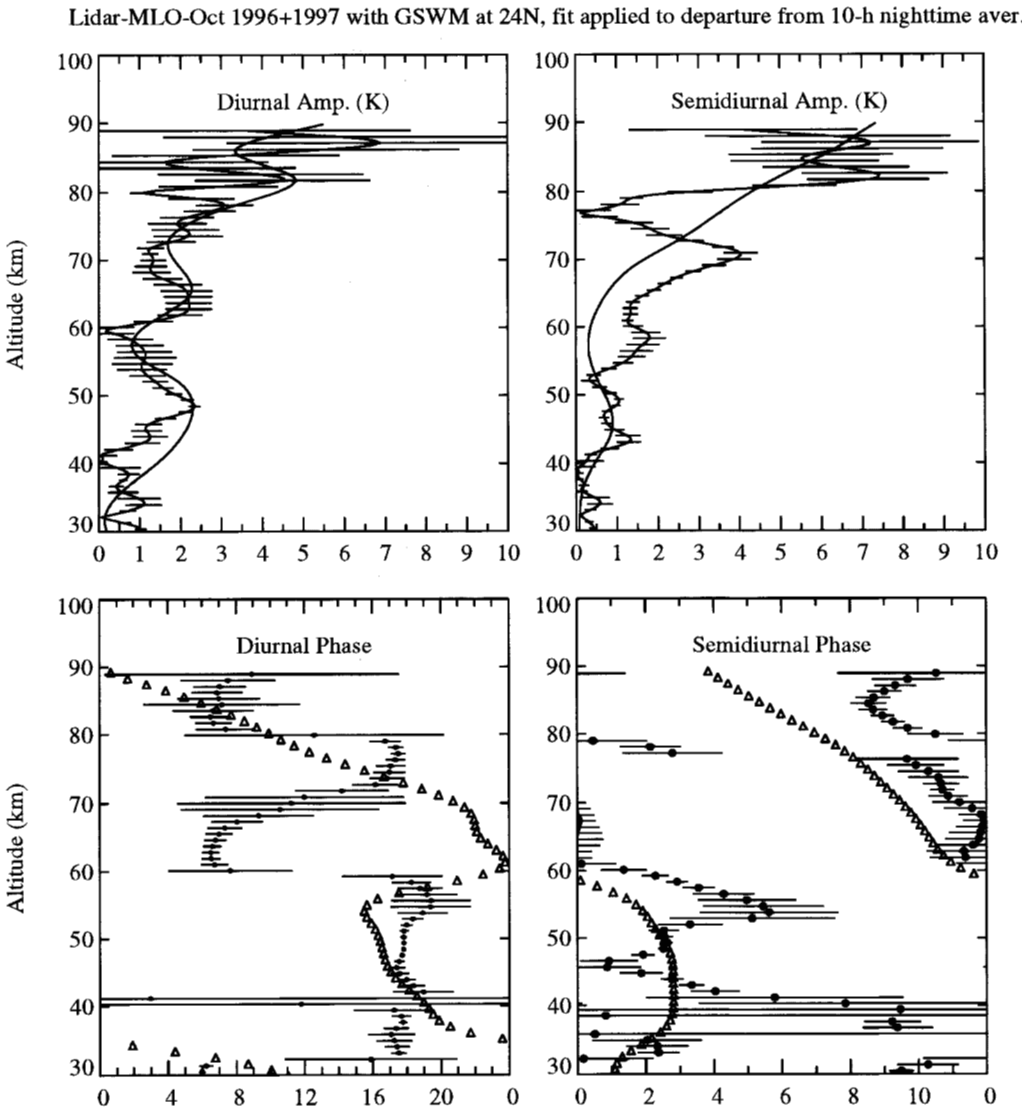

Figure 9. Same as figure 5, but with the phases and amplitudes predicted by GSWM at 24°N.

ACKNOWLEDGEMENTS

The work described in this paper was carried out at the Jet Propulsion Laboratory, California Institute of Technology, under an agreement with the National Aeronautics and Space Administration. We are grateful to Maura Hagan (NCAR) for helpful discussions regarding GSWM.

REFERENCES

1. S. Chapman, and R. S. Lindzen, "Atmospheric tides", pp. 1-201, D. Reidel, Norwell, Mass., 1970.
2. J. M. Forbes, "Atmospheric tides 1. Model description and results for the solar diurnal component", *J. Geophys. Res.*, **87**, pp. 5222-5240, 1982.
3. J. M. Forbes, "Tidal and planetary waves, The upper mesosphere and lower thermosphere: A review of experiment and theory", Geophysical Monograph 87, pp. 67-87, 1995.
4. M. D. Burrage, R. A. Vincent, H. G. Mayr, W. R. Skinner, N. F. Arnold and P. B. Hays, "Long-term variability in the solar diurnal tide observed by HRDI and simulated by the GSWM", *Geophys. Res. Lett.*, **22**, pp. 2641-2644, 1995.

5. B. V. Khattatov, V. A. Yubin, M. Geller, P. B. Hays and R. A. Vincent, "Diurnal migrating tide as seen by the high-resolution Doppler imager/UARS 1. Monthly mean global meridional winds", *J. Geophys. Res.*, **102**, pp. 4405-4422, 1997.
6. A. H. Manson, C. E. Meek, H. Teitelbaum, F. Vial, R. Schminder, D. Kuschner, M. J. Smith, G. J. Fraser, and R. R. Clark, "Climatologies of semi-diurnal and diurnal tides in the middle atmosphere (70-110 km) at middle latitudes (40-55°)", *J. Atmos. Terr. Phys.*, **51**, pp. 579-593, 1989.
7. C. McLandress, G. G. Shepherd and B. H. Solheim, "Satellite observations of thermospheric tides: Results from the Wind Imaging Interferometer on UARS", *J. Geophys. Res.*, **101**, pp. 4093-4114, 1996.
8. T. Leblanc, I. S. McDermid, and D. A. Ortland, "Lidar observation of the middle atmospheric thermal tides. Comparison with HRDI and GSWM. Part I: Methodology and winter observations over Table Mountain (34.4°N)"., *J. Geophys. Res.*, (submitted), 1998.
9. I. S. McDermid, T. D. Walsh, A. Deslis and M. L. White, "Optical systems design for a stratospheric lidar system", *Appl. Opt.*, **34**, pp. 6201-6210, 1995.
10. D. A. Ortland, P.B. Hays, W.R. Skinner and J.-H. Yee, "Remote sensing of mesospheric temperature and $O_2(^1\Sigma)$ band volume emission rates with the high-resolution Doppler imager", *J. Geophys. Res.*, **103**, pp. 1821-1835, 1998.
11. M. E. Hagan, J. M. Forbes and F. Vial, "On modeling migrating solar tides", *Geophys. Res. Lett.*, **22**, pp. 893-896, 1995.
12. T. Leblanc, T., I. S. McDermid, A. Hauchecorne, and P. Keckhut, "Evaluation and optimization of lidar temperature analysis algorithms using simulated data", *J. Geophys. Res.*, **103**, pp. 6177-6187, 1998.
13. P. D. Dao, R. Farley, X. Tao, and C. S. Gardner, "Lidar observations of the temperature profile between 25 and 103 km: evidence of strong tidal perturbation", *Geophys. Res. Lett.*, **22**, pp. 2825-2828, 1995.
14. J. M. Forbes, M. E. Hagan, X. Zhang, and K. Hamilton, "Upper atmosphere tidal oscillations due to latent heat release in the tropical troposphere", *Ann. Geophys.*, **15**, pp. 1165-1175, 1997.